Article

Large-Scale Ejecta of Z CMa—Proper Motion Study and New Features Discovered

Tiina Liimets [1,*], Michaela Kraus [1], Lydia Cidale [2,3], Sergey Karpov [4] and Anthony Marston [5]

1   Astronomical Institute, Czech Academy of Sciences, Fričova 298, 25165 Ondřejov, Czech Republic
2   Instituto de Astrofísica de La Plata (CCT La Plata-CONICET, UNLP), Paseo del Bosque S/N,
    La Plata B1900FWA, Buenos Aires, Argentina
3   Departamento de Espectroscopía, Facultad de Ciencias Astronómicas y Geofísicas, Universidad Nacional
    de La Plata, Paseo del Bosque S/N, La Plata B1900FWA, Buenos Aires, Argentina
4   Institute of Physics of the Czech Academy of Sciences (FZU AV ČR), Na Slovance 2,
    Praha 8, 18200 Prague, Czech Republic
5   European Space Agency, European Space Astronomy Centre, Camino Bajo del Castillo, s/n Urbanización
    Villafranca del Castillo Villañueva de la Cañada, E-28692 Madrid, Spain
*   Correspondence: tiina.liimets@asu.cas.cz

Abstract: Z Canis Majoris is a fascinating early-type binary with a Herbig Be primary and a FU Orionis-type secondary. Both of the stars exhibit sub-arcsecond jet-like ejecta. In addition, the primary is associated with the extended jet as well as with the large-scale outflow. In this study, we investigate further the nature of the large-scale outflow, which has not been studied since its discovery almost three and a half decades ago. We present proper motion measurements of individual features of the large-scale outflow and determine their kinematical ages. Furthermore, with our newly acquired deep images, we have discovered additional faint arc-shaped features that can be associated with the central binary.

1. Introduction

Z Canis Majoris (Z CMa) has intrigued astronomers for decades. It is an active early-type emission line binary consisting of a Herbig Be primary and a FU Orionis-type (FU Ori) secondary separated by 0″.1 (e.g., Bonnefoy et al. [1]). Current high-spatial resolution observations show that the primary is located in the northwest (NW) direction from the secondary (e.g., Bonnefoy et al. [1]; Dong et al. [2]). The light curve of the system is rich in long-term variability, months to years, as well as in day-by-day variability with a non-periodic nature and varying amplitudes (Sicilia-Aguilar et al. [3] and references therein).

The system is surrounded with multiple circumstellar and large-scale outflows. The brightest feature around Z CMa is a reflection nebula extending up to about 35″ toward the NW from the central binary. It was discovered from photographic plates from 1953 by Herbig [4]. On these plates, the reflection nebula has a bar-shaped morphology (see Figure 10 in Herbig [4]). However, on the newer, higher resolution and more sensitive CCD images, the morphology more closely resembles a comma (Figure 1 left and Figure 2). We refer to this feature as comma nebula.
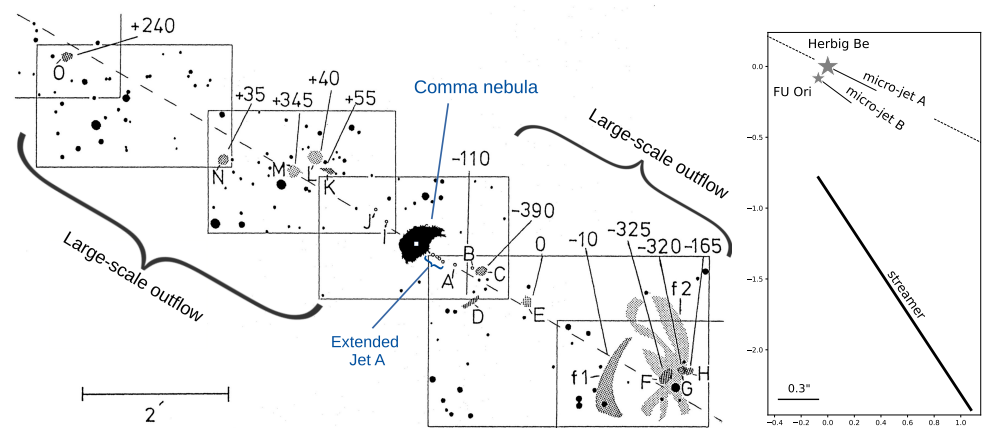
Figure 1. (**Left**): Schematic view of the various extended nebular features surrounding Z CMa. The stars in the field of view are drawn as black filled circles, large-scale outflow features are marked with grayish areas or circles with black contures. The dashed line is drawn at the 60° position angle. Individual numbers refer to radial velocities (Poetzel et al. [5]). Field of view is $9'.5 \times 5'.6$. The base of the figure is depicted from Poetzel et al. [5]. Reproduced with permission © ESO. (**Right**): Schematic view of the sub-arcsecond features around Z CMa presented in true proportions. The lengths of the micro-jets are taken from Whelan et al. [6] and those for the streamer are taken from Dong et al. [2]. The dashed line represents the position angle of the large-scale outflow. Field of view is $1''.6 \times 2''.7$. A white square representing the same size is drawn on the left panel at the position of the central binary inside the comma nebula. On both panels, north is up and east is to the left.
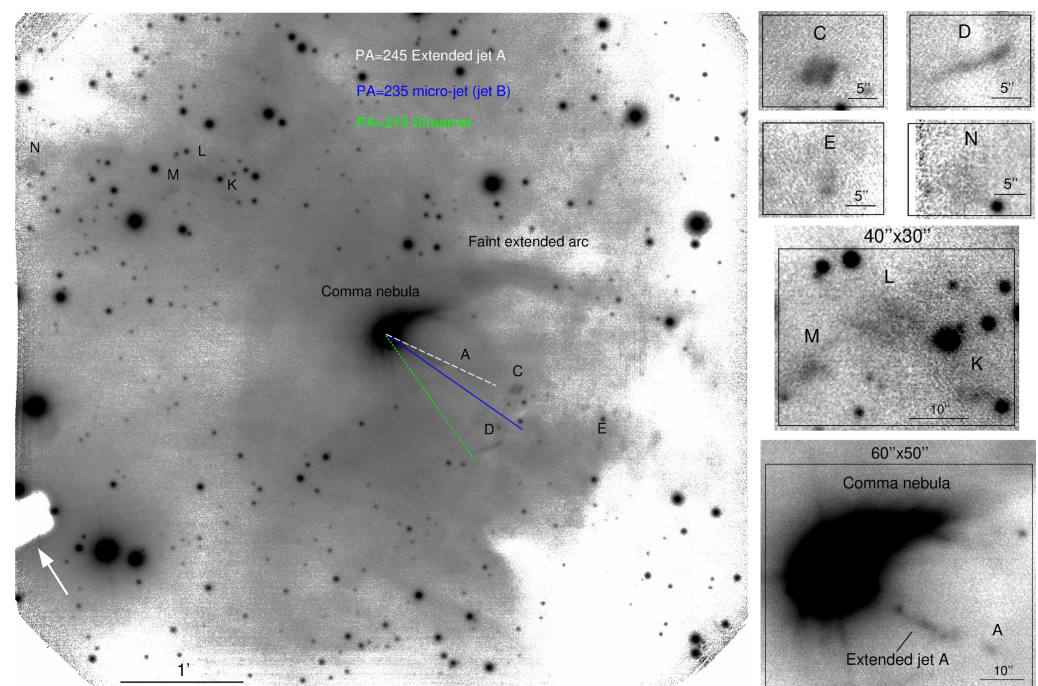
Figure 2. (**Left**): [S II] image of Z CMa acquired with GMOS attached to Gemini-South. The white square shape feature, indicated with a white arrow, is an artifact from vignetting of the guiding probe. (**Right**): Insets of the resolved features in the [S II] image. The FOVs of the smallest insets are $20'' \times 15''$ each. On all images, north is up, east is to the left, and the intensity is in log scale to improve the contrast. See text for more details.

In the sub-arcsecond scale, jets emerge from both components—micro-jet A from the primary and micro-jet B from the secondary at the position angle (PA, measured from north to east) 245° and 235°, respectively (Whelan et al. [6]; Figure 1 right). Both jets are

slightly wiggly and show associated knots (Whelan et al. [6]; Antoniucci et al. [7]). The micro-jet A extends out to about 30″ and is referred to as (extended) jet A (Figure 1 left) in the literature. This jet was discovered by Poetzel et al. [5], and it has also a wiggly nature (Whelan et al. [6]).

Millan-Gabet and Monnier [8] discovered another jet-like small-scale feature at PA 215°. This feature is designated in the literature as a streamer, and its length is about 2″ (Figure 1 right). However, it does not emanate from either of the binary components. In fact, it appears to start 0″.7 toward the south (S) from the central binary (Dong et al. [2]). The same authors find a point source a further ∼2″ away from the streamer at the same PA and therefore confirm that the streamer is most likely created in a rare flyby event. Furthermore, these authors point out that the flyby event explains also the anomalous double-jet activity in this system, which considering the masses of the binary components could happen only with the probability of less than 1%.

Looking at greater distances, further out from the extended jet A at the same PA, a large-scale outflow was discovered by Poetzel et al. [5] from the narrow-band Hα and [S II] images acquired in the end of 1990s. While the micro and extended jets are primarily detected as one-sided objects in the southwest (SW) direction, the large-scale outflow has emission features also toward the northeast (NE) (Figure 1 left). The large-scale outflow consists of blobby and elongated features. The kinematics of the features refer to a bipolar nature.

The NE features are all red-shifted, while the SW ones appear blue-shifted. Eight features are identified by Poetzel et al. [5] in the SW side extending up to 4′.7 and seven features are identified in the NE reaching up to 6′ from the central object. This is the largest known outflow[1] for this type of stars extending across 3.5 pc when considering the distance of 1125 pc (Dong et al. [2]). At the discovery years, the average PA of the outflow features was 60° (equivalent to 240°). This PA aligns with that of the extended jet A, which is associated with the primary, and it is therefore widely accepted that the large-scale outflow is a result of the ejections from the Herbig Be component.

The large-scale outflow is what we concentrate on in this paper. In particular, we will measure proper motions of the individual features, and in combination with their respective radial velocities, we aim to reveal the true 3D nature of this huge nebulosity. For that, an accurate distance estimation is essential. Several distance estimates for Z CMa exist in the literature. They are all based on the fact that Z CMa is a member of the OB association CMa OB1. Published values are 1150 ± 50 pc by Clariá [12], 990 ± 50 pc by Whelan et al. [6], and more recently 1125 ± 30 pc by Dong et al. [2]. Throughout this paper, we use the latest estimate, 1125 pc, because it was calculated by using the largest number of members of the association (50) and is therefore the most accurate one. We note here that the estimated Gaia Data Release 3 (Gaia DR3) (Gaia Collaboration et al. [13]; Gaia Collaboration et al. [14]) distance of the Z CMa is not reliable due to the very large value of RUWE[2], as described in Dong et al. [2].

2. Observations and Data Reduction

Our first imaging data were obtained with the 60-inch telescope at Mt. Palomar on 2002 February 28. A single 20-min exposure in a narrow-band Hα filter ($\lambda = 6564.8$ Å, $\Delta\lambda = 20$ Å) was secured with a seeing of 1″.5. The field of view (FOV) was 12′.5, and a chosen binning of 2×2 provided a pixel scale of 0″.756 pix^{-1}. This image was reduced using the standard routines in IRAF[3] (Tody [15,16]).

The second set of images of Z CMa was acquired on 2019 September 27 with the 8.1 m telescope. We used the Gemini Multi-Object Spectrographs (GMOS, Hook et al. [17]) mounted at Gemini-South as part of the observing proposal AR-2019B-020. The images were collected in the narrow band Hα G0336 ($\lambda = 6567.0$ Å, $\Delta\lambda = 70$ Å) and [S II] G0335 ($\lambda = 6717.2$ Å, $\Delta\lambda = 43$ Å) filters with the total exposure time of 145 and 435 s, respectively. The observations in both filters consisted of several shorter exposures that have been dithered to eliminate the gaps between the detectors and to minimize contamination (saturation effects) due to the bright central star. The bin 2×2 was used, yielding a pixel

scale of $0''.16$ pix^{-1}. The FOV of the final reduced images is $6' \times 5'.5$. The observations were carried out with a seeing between $1''.3$ and $1''.4$. Data reduction was performed using the Gemini software DRAGONS (Labrie et al. [18]). Details of the observations are in Table 1.

Table 1. Log of the observations. The first column lists the start date of the observing night. Column 2 lists the telescope used. Column 3 contains the central wavelength (λ) and the width ($\Delta\lambda$) of the filter. The last column is the total exposure time in seconds.

Date	Telescope	Filter $\lambda/\Delta\lambda$ (Å)	Total Exp. Time (s)
28 February 2002	60-inch Mt. Palomar	Hα 6564.8/20	1200
27 September 2019	Gemini-South	Hα 6567.0/70	145
27 September 2019	Gemini-South	[S II] 6717.2/43	435

We also acquired a set of stacked images from the Pan-STARRS images archive (Waters et al. [19]) that are results of co-adding multiple exposures made between 2010 and 2015 during the 3π survey (Chambers et al. [20]). We downloaded stacked images covering the region around Z CMa in g, r, i, and z filters, re-scaled them to the common photometric zero point, and created mosaics in each individual filter with the original spatial resolution of the Pan-STARRS stacked images of $0''.25$ pix^{-1}. We then created a composite RGB image from z, i, and g mosaics with logarithmic intensity scaling applied. We excluded the r filter from the composite image as it shows the largest number of stacking artifacts in the background, and it is mostly unusable for studying the morphology of the nebular features. The FOV of the final image was $9' \times 9'$.

2.1. Pre-Analysis Processing of the Narrow-Band Images

To accurately analyze the possible morphological and/or kinematical changes between our two epochs, our narrow-band Hα images first had to be matched pixel by pixel. For this, we used 32 stars in the FOV whose proper motions were smaller or equal to ±5 mas year^{-1} and RUWE < 1.4; all values were taken from the Gaia DR3. The 2019 frame was matched against the 2002 frame, because the latter had a larger pixel scale. The matching was completed in IRAF using the tasks *geomap* and *geotran*. The errors of the matching were $\sigma_{RA} = 0''.18$ and $\sigma_{DEC} = 0''.23$. With this procedure, both frames were given the same pixel scale, $0''.756$ pix^{-1}. The last step in matching the coordinates is to compensate for the possible proper motion of the central star. In our case, this effect is insignificant, considering the small proper motion of Z CMa (see Section 3.4) and that our two datasets are separated by 17.58 years. In this stage of the image processing, the frames were ready to be compared by blinking to find any obvious movement of the outflow features in the plane of the sky or to measure directly the coordinates of individual features to calculate proper motions.

For the features for which the blinking of the frames did not reveal any visual expansion and/or which, due to their elongated shape, are not suitable for direct coordinate measuring, further processing was needed in order to use the magnification method (see Section 3.2). These steps included seeing and flux matching. The first was not needed because the seeing of the original frames was already similar, and after pixel by pixel matching, it became equal. Flux matching was completed using the analyzed feature (in our case feature D; see Section 3.2) by summing up all the flux in a rectangle-shaped area equivalent to the size and shape of the feature and then arithmetically matching it with the same area flux on the second epoch image. Beforehand, the sky was removed. We estimate that the flux matching is accurate down to a few percent.

3. Results

In Figure 3, we present our 2002 Hα image which covers the whole large-scale outflow of Z CMa, extending $10'.7$ from NE to SW. Our GMOS images from 2019 have a smaller FOV as demonstrated with the black rectangle in Figure 3. The GMOS image taken in the lines of [S II] $\lambda\lambda6716$, 6731 is considerably deeper and presents the individual features

with a better S/N (Figure 2). For a meaningful analysis (see Sections 3.1 and 3.2), it is important to use data in the same filter/spectral lines, especially when the aim is to find any morphological and/or kinematical changes between two epochs. The reason is that the excitation of emission lines from diverse elements can occur under different physical conditions so that the lines do not necessarily trace the same gaseous regions. Therefore, we restrict our proper motion analysis to the Hα frames, because we do not have a [S II] frame from 2002. In addition, our two Hα frames have a similar S/N, hence presenting similar detectability of the features, further making them a suitable match for the analysis. However, we note here that all the features that are resolvable in the GMOS Hα frame have the same morphology and position in the GMOS [S II] frame.
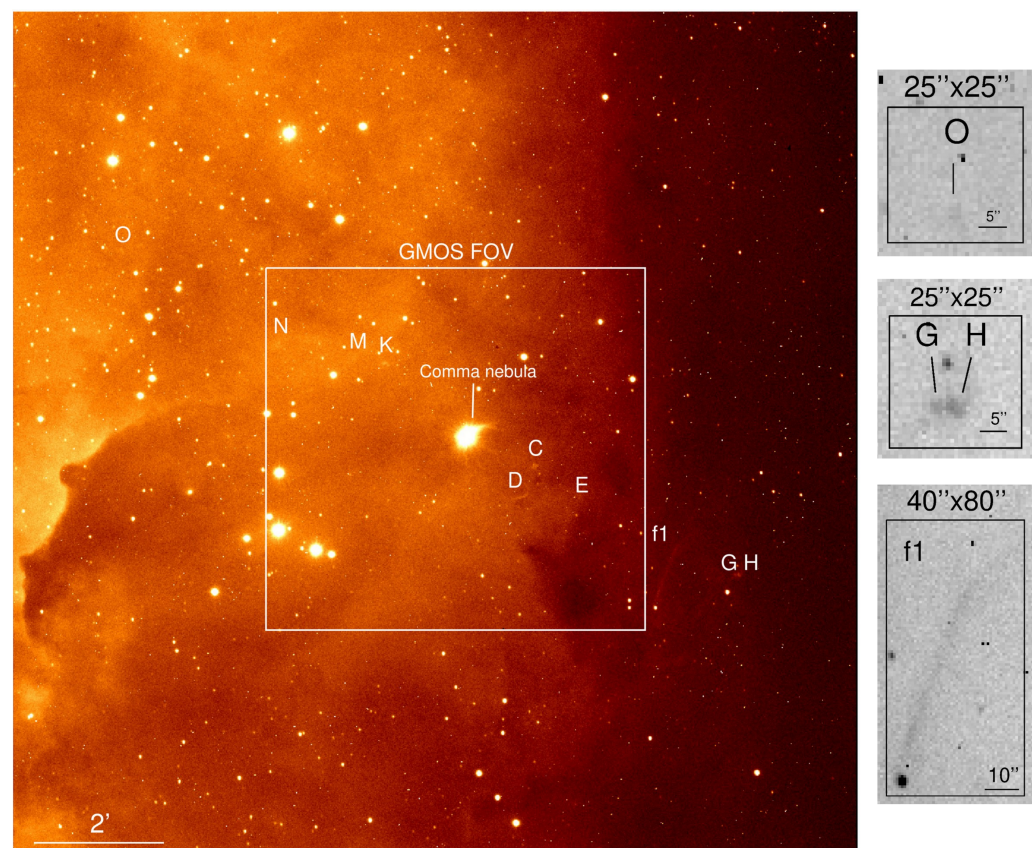
Figure 3. (**Left**): Hα image of Z CMa taken in 2002. GMOS FOV is shown for comparison. (**Right**): Insets of the features resolvable in the Hα image and which are outside GMOS FOV. On all images, north is up, east is to the left, and the intensity is in log scale to improve the contrast. See text for more details.

We refer to the individual features as they have been named by previous authors. The features of the large-scale outflow were named by Poetzel et al. [5] using capital letters from *A* to *O* (Figure 1). In addition, the designation of *f*1 and *f*2 was given to refer to the filaments in the SW side nearby the blobby features *F*, *G*, and *H*. On our figures, the labels of the features are always directly above the feature itself, apart from the label *f*1 which is to the left from the feature (Figure 3). We note here that not all the features presented by Poetzel et al. [5] are detectable and/or resolvable in our 2002 Hα frame due to the slightly lower S/N. From our GMOS [S II] frame, we could identify the features *A*, *B*, *C*, *D*, *E*, *M*, *N*, *K*, and *L*. Features *O*, *G*, *H*, and *f*1 are outside the GMOS FOV. We could not identify features *I* and *J*, situated between the central star and the feature *K*, on any of our images, which is probably due to a slightly lower S/N of our images compared to the images from Poetzel et al. [5].

The morphology of the large-scale outflow has not changed during the past 30 years when comparing our 2019 image with the 2002 one and the one from 1988–1989 from Poetzel et al. [5] (compare their Figure 1 with our Figures 2 and 3). The large-scale outflow has a bipolar nature and it consists of individual features (features *A* to *O*) with varying shapes—blobby, elongated, filamentary, arced. The PA of the outflow is ∼60° (or ∼240°), as measured from our images. The approximate value is due to the slightly different PAs of individual features. Nevertheless, this shows that the PA of the outflow has not changed during the past 30 years either (∼60° is measured also by Poetzel et al. [5]).

In our [S II] frame (Figure 2), we refer to a few other features related to the ejections from Z CMa: in particular, the extended jet A (see also Figure 3 in Whelan et al. [6]), the PA of the micro-jet B (see also Figure 1 in Antoniucci et al. [7]), and the PA of the streamer (see also Figure 2 in Canovas et al. [21]). Figure 2 shows also the previously known bright comma nebula which is almost perpendicular to the large-scale outflow. Furthermore, our image reveals another, fainter and previously not detected extended arc-shaped feature in the NW direction, which will be discussed further in Section 3.4 and 4.

As a first step in finding any expansion in the plane of the sky, we have used the simple blinking of the two Hα matched frames. It reveals that feature *C* has a visible expansion, while the rest of the features appear to stand still. Overall, a reliable analysis is only possible for the brightest features, which are those labeled with *C* and *D*. Therefore, we focus in the following on these two and determine their proper motions before we take a closer look at the faint arc structures.

3.1. Proper Motion Calculations of Feature C

Feature *C* is one of the brightest among the large-scale outflow. It has a roundish shape and is clearly detectable in both of our Hα frames taken in 2002 and 2019. The exact temporal separation of the two images is 17.58 years. The shape of feature *C* does not change during that period. As mentioned above, feature *C* presents the fastest motion from the central star compared to other features. In addition, feature *C* also has the largest radial velocity compared to other features as measured by Poetzel et al. [5]. Therefore, considering the inclination angle out of the plane of the sky (see below), it is not surprising that this feature would show a clear expansion in the plane of the sky while others do not. The movement in the plane of the sky of feature *C* is in accordance with the general direction of the features in SW direction, confirming that it must have been ejected from Z CMa.

Due to the roundish shape of feature *C*, it was possible to measure directly its central coordinates on both of our images. The total movement in the plane of the sky during the 17.58 years considered is $1''.4$, yielding a proper motion of $0''.08$ year^{-1} and a tangential velocity of ∼420 km s^{-1}. Considering the radial velocity of -390 km s^{-1} of feature *C* (Poetzel et al. [5]), its expansion velocity is about 580 km s^{-1} and the inclination out of the plane of the sky is 43° using the ordinary cosine relation between the velocity vectors ($i = arccos(v_{sky}/v_{exp})$). The found inclination angle agrees with the estimates made for the micro-jet B, which was proposed to have an inclination angle between 28° and 64° (Antoniucci et al. [7]) according to the tangential and radial velocity estimates by Whelan et al. [6].

The distance of feature *C* from the central star is $68''$ and $69''$ during the observations taken in 2002 and 2019, respectively. The position angle of feature *C* has not changed during the time duration between our 2002 and 2019 images, and it is 246°. Precise measurements with errors for all the calculated values are in Table 2.

Table 2. Results of the calculations from direct measuring of feature *C* and from using the magnification method for feature *D*. A distance of 1125 pc toward Z CMa was adopted. See text for more details.

Description	Feature *C*	Feature *D*
Total movement in the plane of the sky ($''$)	1.4 ± 0.3	-
Proper motion μ ($''$ year^{-1})	0.08 ± 0.02	0.013 ± 0.004
Radial velocity [a] v_{rad} (km s^{-1})	-390 ± 24	-110 ± 24
Tangential velocity v_{sky} (km s^{-1})	423 ± 88	69 ± 23
Expansion velocity v_{exp} (km s^{-1})	576 ± 67	130 ± 24
Inclination out of the plane of the sky i (°)	43 ± 15	58 ± 14
Distance from the central star in 2002 d_{2002} ($''$)	67.8 ± 0.3	75.3 ± 0.8
Distance from the central star in 2019 d_{2019} ($''$)	69.2 ± 0.3	75.5 [b] ± 0.8
PA at 2002 (°)	246.5 ± 0.2	222.9 ± 0.6
PA at 2019 (°)	246.6 ± 0.2	222.9 ± 0.6
Age at 2002 (years)	854 ± 177	5859 ± 1953
Magnification factor M	-	1.003 ± 0.001

[a] From Poetzel et al. [5]. [b] Calculated from d_{2002} and our derived proper motion.

Using the above calculated proper motion, the distance from the central star, and assuming constant expansion velocity since the ejection, it is possible to calculate the age of feature *C* at our first epoch, 2002. It is on the order of 850 years, which is in accordance with the estimates in Poetzel et al. [5].

3.2. Proper Motion Calculations of Feature D

The second feature for which we were able to calculate the expansion in the plane of the sky is the arc-shaped feature *D*. Due to its elongated shape, a direct measuring of the coordinates was not an appropriate method. For that reason the magnification method (see, e.g., Santander-García et al. [22]; Liimets et al. [23]) was used, which is suitable to find the proper motion of extended structures without a clear central point and/or when the total movement in the plane of the sky is as small as a tenth of a pixel. Both criteria are valid for feature *D*. The magnification method is based on finding a magnification factor *M*, which represents an image with minimum residuals of the magnified first epoch image, which is subtracted from the second epoch image. The method provides the proper motion, tangential velocity, and age. In order to use the magnification method, the frames being analyzed have to have coordinates, seeing, and flux matched. This was completed using the procedures described in Section 2.1. Further details about the magnification method and the derivation of the formulas used in the following can be found in Section 3.3 of the PhD thesis by Liimets [24]. The best magnification factor for feature *D* was determined to be $M = 1.003 \pm 0.001$. However, we note here that this result should be used with caution. We can say with confidence that *M* is not larger than 1.003. Consequently, all the following numerical values should be taken as upper limits. The proper motion can be calculated, in convenient units, in the following way

$$\mu[''\text{year}^{-1}] = \frac{(M-1) \cdot d['']}{\Delta t[\text{year}]}, \tag{1}$$

where *d* is the distance of feature *D* from the central star on the first epoch, in our case the year 2002, and Δt is the time interval between the two epochs. In the case of the elongated feature *D*, the distance from the central star is somewhat challenging to estimate. However, we are confident that when considering a somewhat larger error of 1 pixel, it is accurate enough to serve the purpose of the simple calculations presented in this paper. Hence, the distance of feature *D* from the central star at our 2002 epoch is $75'' \pm 1''$, and considering Equation (1), the proper motion becomes $\mu = 0''.013$ year^{-1}. As for feature *C*, the precise values with their errors for all the calculations for feature *D* are in Table 2.

Using the proper motion and the distance to feature *D*, it is possible to calculate the tangential velocity in the following convenient units

$$v_{sky} \; [\text{km s}^{-1}] = 4.74 \cdot \mu \; [''\; \text{year}^{-1}] \cdot D \; [pc]. \tag{2}$$

We consider the distance to Z CMa to be 1125 pc and therefore $v_{sky} = 69 \text{ km s}^{-1}$. The radial velocity of feature D has been measured to be -110 km s^{-1} (Poetzel et al. [5]), which results in an expansion velocity of 130 km s^{-1}. The inclination angle would therefore be slightly larger than for feature C but with a value of 58° again matching with the estimates in Antoniucci et al. [7].

The magnification factor can also be used to calculate the age of the feature at the first epoch,

$$T \; [\text{year}] = \frac{\Delta t \; [\text{year}]}{(M-1)}, \tag{3}$$

which for feature D gives a value of about 6000 years.

The PA of feature D is constant between our two observing epochs and has a value of 223°.

3.3. Proper Motion of Other Features

We tried to measure the expansion in the plane of the sky for the two other features, E and K, which were considerably fainter than the features C and D but still resolvable compared to the rather marginal detections of the features L, M, and N. Features E and K have an irregular shape, and therefore, the magnification method was used. We find no measurable movement in the plane of the sky for both features. For feature E, it is somewhat expected due to its RV being 0 km s^{-1} (Poetzel et al. [5]), while the RV of feature K is quoted as +55 km s^{-1} by the same authors. Considering the pixel scale of $0''.756$ of our matched images and the fact that the magnification method is able to measure an expansion of about one tenth of a pixel, the smallest tangential velocity that we should be able to detect is $\sim$20 km s^{-1}. This, in return, would mean an inclination out of the plane of the sky 70°, which, within our error estimate of ±10°, agrees with the estimates by Antoniucci et al. [7].

3.4. Faint Extended Arc

From our deep GMOS [S II] image, we have discovered that the bright comma nebula has a fainter continuation. We designate this feature a faint extended arc (see Figure 2). Despite the lower S/N of our GMOS Hα image, the faint arc is also detectable on that frame, but we refrain from showing it because it does not provide new information. With an orientation of the faint arc toward the NW, it is perpendicular to the main large-scale outflow. The arc is more pronounced on the Pan-STARRS RGB image (Figure 4) on which additional related features become visible. We detect a repeating pattern of filaments, inside the main arc, which seem to mimic "feathers" (see white arrows in Figure 4). Interestingly, while most of the feathers do not have a direct connection to the star, the closest feather to the central binary, designated with number 1, seems to have connecting filaments. These filaments start from the bright comma nebula as a small arc resembling a "fishtail" (marked with solid red arrow) and then continue toward feather 1 with less homogeneous emission. From the image, it is visible that the diffuse emission in the direction of feather 2 is continuous further than that of our Pan-STARRS FOV. However, the faint extended arc which ends with feather 4 extends up to $3'$ toward the west.
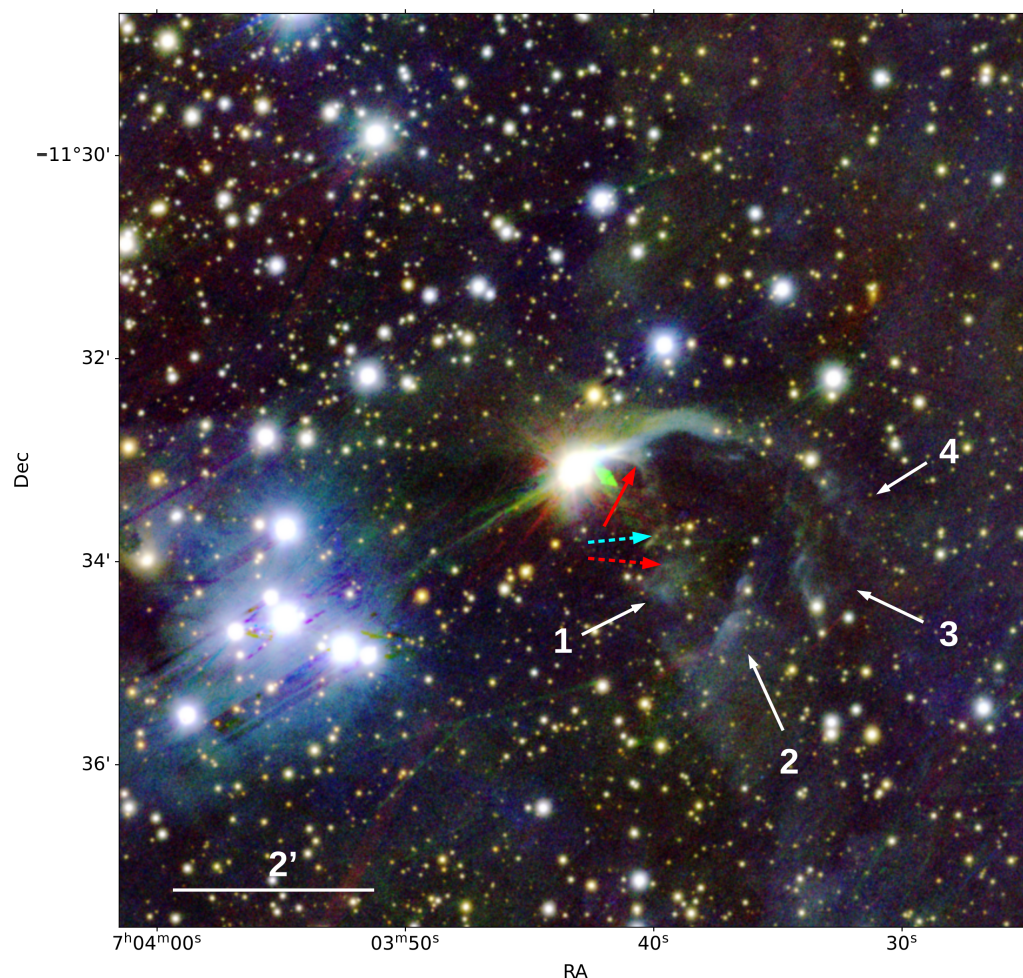
Figure 4. Pan-STARRS RGB image presenting the faint extended features around Z CMa. Red channel corresponds to *z* filter, green channel corresponds to *i*, and blue channel corresponds to *g* filter. The intensity is in log scale to improve the contrast. North is up and east is to the left. FOV $9' \times 9'$. See text for more details.

4. Discussion

Looking at the Figure 4, it is tempting to assume that the newly discovered faint extended features, as well as the bright comma-shaped feature, are created by matter expelled from the central star during a single or multiple independent mass ejection event(s) and now appear misplaced from the central position of the object due to the movement of Z CMa through the interstellar medium. However, the proper motion of the star, $\mu_{RA} = -4.4$ mas year^{-1} and $\mu_{DEC} = 2.0$ mas year^{-1} (Hipparcos-2 catalog, van Leeuwen [25]), does not support that. Z CMa is moving toward the faint extended arc and not away from it. Our choice of using the proper motion values from the Hipparcos-2 catalog is due to the mentioned large RUWE value of Z CMa in Gaia DR3 (see Section 1), referring to a problematic astrometric solution. The latter is most probably a result of the binary nature of the object and its generally rather bright photometric values. However, we note that Gaia DR3 proper motion values agree relatively well with the Hipparcos-2 catalog.

Another possibility, due to the roundish shape, is that the faint extended arc with the feathers is related to the orbital motion of the binary. Considering the recent high-contrast imaging polarimetry observations (Canovas et al. [21]), the orbital movement of the FU Ori companion around the primary is $0°.7$ year^{-1} when considering a circular orbit. This implies an orbital period of about 500 years. Currently, the FU Ori companion is located in the southeast (SE) direction from the primary (e.g., Figure 2 in Bonnefoy et al. [1]). Therefore, considering the hypothesis of a single ejection and the position of the faint

extended arc and its feathers, they could have been ejected half a period ago. However, taking into account the distance of these features from the central binary, it would imply a peculiarly large tangential velocity of $\sim$3700 km s^{-1}, which has not been measured in any other features related to the small- or large-scale outflows of Z CMa. The obvious repeating pattern of the feathers could also suggest consecutive mass ejections occurring on every orbit at a specific location. We can then assume that the closest feather could have been ejected half a period ago and the next ones could have been ejected 1.5, 2.5, and 3.5 periods ago, respectively. The equivalent tangential velocities would then be about 1800, 900, 600, and 530 km s^{-1}, considering distance estimates for each feather from the central binary of 85, 130, 148, and 180″, respectively. While the radial velocities of -600 km s^{-1} have been measured to be associated with the micro-jets (Poetzel et al. [5]; Whelan et al. [6]), all these estimated values exceed our measured tangential velocities of the large-scale outflow features (see Table 2). If we consider our largest tangential velocity of 420 km s^{-1}, and the largest extent of the faint arc structures (3′), it would have had to be ejected $\sim$2300 years ago. This timescale is comparable with the ages we have found for the large-scale outflow features *C* and *D*, 850 and 5900 years, respectively. However, if these newly discovered features are related to the mass ejections occurring at the particular location during the orbit of the FU Ori-type companion around the primary, it is more likely that the orbit is not circular but elliptical. The latter would include periastron passage, which can enhance the mass-loss and possibly initiate outflows, as has been seen in other binary systems (e.g., in a case of symbiotic binary R Aquarii (Liimets et al. [26]) and proposed for the formation of the circumbinary molecular ring in the B[e] supergiant system GG Car (Kraus et al. [27])). At the same time, while feathers 2 and 3 do not seem to be physically connected with the central binary, the faint extended arc and its extension feather 4 are clearly a continuation from the star and its bright comma nebula, implying a constant flow of matter. At this point, we also mention that when inspecting the Figure 4 more thoroughly, it is possible that there is a dark cloud blocking the connections of the feathers with the central binary or with the faint arc, as there are no stars detected in the west from the binary below the faint arc. However, according to the study based on 2 Micron All Sky Survey by Dobashi [28], there are no dark clouds in the FOV of our Figure 4.

We can further calculate the possible tangential velocities related to the new discovered features when considering their maximum extent of 3′ and the ages found for the features *C* and *D*. The age of 850 years would result in a velocity of about 1100 km s^{-1}, while the 5900 years (feature *D*) would result in a velocity of about 160 km s^{-1}. The latter is more in line with the tangential velocities measured in this work and with the radial velocities measured by Poetzel et al. [5]. It is possible that the elongated feature *D*, which indeed has a larger deviation from the average PA of the large-scale outflow compared to other features, potentially referring to a different origin, is related to the feather 1. However, the seemingly similarly shaped feature marked with dashed cyan arrow in Figure 4 is not feature *D*. Feature *D* is 15″ further away from the central star and has a slightly smaller PA. A red dashed arrow is indicating its position in Figure 4, and it shows that this feature is situated on the edge of the feather 1, but there is no brightness enhancement in that position other than the boarder line of the feathery feature.

On the other hand, it cannot be ruled out that the faint features are accidentally aligned with Z CMa and that they are actually part of the huge nebula Sh 2-296 on which edge Z CMa is located (see Figure 6 in Fernandes et al. [29]). However, due to the obvious positional proximity to Z CMa, we are inclined to favor the idea that the discovered features are connected to Z CMa rather than being aligned by chance.

The new detected faint features as well as our measured different ages of different features (850 versus 5900 years for feature *C* and *D*, respectively) are in accordance with the nature of the Z CMa binary, which has had several eruptions in the past. The knotty nature of the large-scale outflow as well as the (micro) jets (e.g., Whelan et al. [6], Antoniucci et al. [7]) additionally refer to several discrete mass ejections. In addition, the RVs of the individual features vary a lot with values reaching up to $\sim\pm400$ km s^{-1}

(Poetzel et al. [5]), further supporting the scenario that the central object has experienced in the past several mass ejections with different initial velocities.

Another possible explanation could be that the measured tangential velocities of feature *C* and *D* have not been constant since their ejection from the central binary, which, in return, would affect the calculated ages. However, observationally, we cannot assess it at this point. We have not found suitable observational data prior to 2002 to check the potential velocity canges before our first dataset. In addition, considering the measured velocities, we will have to wait for at least another ∼20 years to obtain a new set of observations, which could potentially show a change in tangential velocities. However, independently of the two scenarios, we wish to emphasize that our measured ages are more precise than previous estimates (Poetzel et al. [5]) because we have accurately measured the tangential velocities, while formerly, those were approximated according to the radial velocities and the possible inclination angle of the large-scale outflow.

As measured from our 2002 and 2019 images, the PA of feature *D* is 223° and does not change during our observing period, 17.58 years. To expand the epoch of analsyis, we estimate from the schematic Figure 1 in Poetzel et al. [5] (they do not publish any numerical values of the PAs nor the distances from the central star) that the PA of feature *D* at their observing time between 1989 and 1990 was ∼225°. Therefore, we conclude that the PA of feature *D* has not changed during the past 30 years. Following this result, the claim made by Whelan et al. [6] that feature *D* is related with the micro-jet B (emanating from the FU Ori-type companion with a PA ∼235°, which is indicated with the blue solid line in Figure 2), according to their observations, is not supported by our precise PA measurements.

We investigate further whether feature *D* could be related to the additional sub-arcsecond component emerging from Z CMa, the jet-like structure identified as a streamer (see Figure 3 in Millan-Gabet and Monnier [8], Figure 2 in Canovas et al. [21], Figure 1 in Liu et al. [30], and Figure 1 in Dong et al. [2]). Unfortunately, these authors do not provide any PA measurements for the straight part of the streamer (the outer edge of this feature is slightly curved toward west), but from their figures, we can estimate it to be approximately 215°. We also note that the streamer does not start from the central binary but about 0″.7 straight toward the south from the binary (see Figure 2 in Canovas et al. [21]). We indicate the PA of this feature with the green dotted line in our Figure 2. Even though the angle of the streamer is more similar to the PA of feature *D* than the angle of the micro-jet B is, it is still clearly evident that their PAs do not align. Dong et al. [2] explains the streamer as a result of the flyby event because they discovered a faint component whose PA matches with the one of the streamer. The fact that feature *D* is not aligned with the streamer provides an additional support for the flyby event because it shows that the streamer is not related to any small or large-scale ejecta.

5. Conclusions

We have presented the first proper motion study of features *C* and *D* within the large-scale outflow of Z CMa. The two very different proper motion values obtained for these two features confirm the previous suggestion that the large-scale outflow is a result of several active ejection phases with varying initial velocities in the life of Z CMa. Our precise position angle measurements of the same features reveal that they are not aligned with the feature streamer, providing further support for the occurrence of the flyby event in this complex system.

We have discovered new features most probably related to Z CMa—a faint extended arc with several features mimicking feathers. It is very likely that these features are connected to the central binary and are the result of previous mass ejection(s) possibly related to the orbital motion of the binary system.

Data Availability Statement: Publicly available GMOS-S and Pan-STARRS datasets analyzed in this study can be retrieved from dedicated archives https://archive.gemini.edu/searchform (accessed on 27 February 2023), and https://ps1images.stsci.edu/cgi-bin/ps1cutouts (accessed on 27 February 2023), respectively. The Mt. Palomar image is available from the corresponding author on reasonable request.

Conflicts of Interest: The authors declare no conflict of interest.

Abbreviations

The following abbreviations are used in this manuscript:

Z CMa	Z Canis Majors
FU Ori	FU Orionis
PA	position angle
FOV	field of view

RUWE	renormalized unit weight error
S	south
NW	northwest
NE	northeast
SW	southwest
SE	southeast

Notes

[1] Although evolved massive stars can have nebula exceeding this size by far, such as the huge bipolar nebula of the B[e] supergiant MWC 314 extending across 13 pc (Marston and McCollum [9]; Liimets et al. [10]) as well as the 10 pc size elaborate filamentary structures around the Luminous Blue Variable P Cygni (see Boumis et al. [11] and references therein).

[2] Renormalised Unit Weight Error (RUWE). RUWE is expected to be around 1.0 for sources where the single-star model provides a good fit to the astrometric observations. A value significantly greater than 1.0 (e.g., >1.4) could indicate that the source is non-single or otherwise problematic for the astrometric solution.

[3] IRAF is distributed by the National Optical Astronomy Observatory, which is operated by the Association of Universities for Research in Astronomy (AURA) under cooperative agreement with the National Science Foundation.

References

1. Bonnefoy, M.; Chauvin, G.; Dougados, C.; Kóspál, Á.; Benisty, M.; Duchêne, G.; Bouvier, J.; Garcia, P.J.V.; Whelan, E.; Antoniucci, S.; et al. The 2008 outburst in the young stellar system Z CMa. III. Multi-epoch high-angular resolution images and spectra of the components in near-infrared. *Astron. Astrophys.* **2017**, *597*, A91.
2. Dong, R.; Liu, H.B.; Cuello, N.; Pinte, C.; Ábrahám, P.; Vorobyov, E.; Hashimoto, J.; Kóspál, Á.; Chiang, E.; Takami, M.; et al. A likely flyby of binary protostar Z CMa caught in action. *Nat. Astron.* **2022**, *6*, 331–338. [CrossRef]
3. Sicilia-Aguilar, A.; Bouvier, J.; Dougados, C.; Grankin, K.; Donati, J.F. Reading between the lines. Disk emission, wind, and accretion during the Z CMa NW outburst. *Astron. Astrophys.* **2020**, *643*, A29. [CrossRef]
4. Herbig, G.H. The Spectra of Be- and Ae-Type Stars Associated with Nebulosity. *Astrophys. J. Suppl.* **1960**, *4*, 337. [CrossRef]
5. Poetzel, R.; Mundt, R.; Ray, T.P. Z CMa: A large-scale high velocity bipolar outflow traced by Herbig-Haro objects and a jet. *Astron. Astrophys.* **1989**, *224*, L13–L16.
6. Whelan, E.T.; Dougados, C.; Perrin, M.D.; Bonnefoy, M.; Bains, I.; Redman, M.P.; Ray, T.P.; Bouy, H.; Benisty, M.; Bouvier, J.; et al. The 2008 Outburst in the Young Stellar System Z CMa: The First Detection of Twin Jets. *Astrophys. J.* **2010**, *720*, L119–L124.
7. Antoniucci, S.; Podio, L.; Nisini, B.; Bacciotti, F.; Lagadec, E.; Sissa, E.; La Camera, A.; Giannini, T.; Schmid, H.M.; Gratton, R.; et al. Sub-0.1″ optical imaging of the Z CMa jets with SPHERE/ZIMPOL. *Astron. Astrophys.* **2016**, *593*, L13.
8. Millan-Gabet, R.; Monnier, J.D. Discovery of a Near-Infrared Jetlike Feature in the Z Canis Majoris System. *Astrophys. J.* **2002**, *580*, L167–L170.
9. Marston, A.P.; McCollum, B. Extended shells around B[e] stars. Implications for B[e] star evolution. *Astron. Astrophys.* **2008**, *477*, 193–202. [CrossRef]
10. Liimets, T.; Kraus, M.; Moiseev, A.; Duronea, N.; Cidale, L.S.; Fariña, C. Follow-Up of Extended Shells around B[e] Stars. *Galaxies* **2022**, *10*, 41.
11. Boumis, P.; Meaburn, J.; Redman, M.P.; Mavromatakis, F. A deep mosaic of [O III]5007 Å CCD images of the environment of the LBV star P Cygni. *Astron. Astrophys.* **2006**, *457*, L13–L16. [CrossRef]
12. Clariá, J.J. A study of the stellar association Canis Major OB 1. *Astron. Astrophys.* **1974**, *37*, 229–236.
13. Prusti, T. et al. [Gaia Collaboration]. The Gaia mission. *Astron. Astrophys.* **2016**, *595*, A1.
14. Brown, A.G.A. et al. [Gaia Collaboration]. Gaia Early Data Release 3. Summary of the contents and survey properties. *Astron. Astrophys.* **2021**, *649*, A1.
15. Tody, D. The IRAF Data Reduction and Analysis System. In Proceedings of the 1986 Astronomy Conferences, Tucson, AZ, USA, 1–2 March 1986; Volume 627, p. 733. [CrossRef]
16. Tody, D. IRAF in the Nineties. *Astron. Soc. Pac. Conf. Ser.* **1993**, *52*, 173.
17. Hook, I.M.; Jørgensen, I.; Allington-Smith, J.R.; Davies, R.L.; Metcalfe, N.; Murowinski, R.G.; Crampton, D. The Gemini-North Multi-Object Spectrograph: Performance in Imaging, Long-Slit, and Multi-Object Spectroscopic Modes. *Publ. Astron. Soc. Pacific* **2004**, *116*, 425–440. [CrossRef]
18. Labrie, K.; Anderson, K.; Cárdenes, R.; Simpson, C.; Turner, J.E.H. DRAGONS—Data Reduction for Astronomy from Gemini Observatory North and South. *Astron. Soc. Pac. Conf. Ser.* **2019**, *523*, 321.
19. Waters, C.Z.; Magnier, E.A.; Price, P.A.; Chambers, K.C.; Burgett, W.S.; Draper, P.W.; Flewelling, H.A.; Hodapp, K.W.; Huber, M.E.; Jedicke, R.; et al. Pan-STARRS Pixel Processing: Detrending, Warping, Stacking. *Astrophys. J. Suppl.* **2020**, *251*, 4.
20. Chambers, K.C.; Magnier, E.A.; Metcalfe, N.; Flewelling, H.A.; Huber, M.E.; Waters, C.Z.; Denneau, L.; Draper, P.W.; Farrow, D.; Finkbeiner, D.P.; et al. The Pan-STARRS1 Surveys. *arXiv* **2016**. [CrossRef]
21. Canovas, H.; Perez, S.; Dougados, C.; de Boer, J.; Ménard, F.; Casassus, S.; Schreiber, M.R.; Cieza, L.A.; Caceres, C.; Girard, J.H. The inner environment of Z Canis Majoris: High-contrast imaging polarimetry with NaCo. *Astron. Astrophys.* **2015**, *578*, L1.

22. Santander-García, M.; Corradi, R.L.M.; Whitelock, P.A.; Munari, U.; Mampaso, A.; Marang, F.; Boffi, F.; Livio, M. HST and VLT observations of the symbiotic star Hen 2-147. Its nebular dynamics, its Mira variable and its distance. *Astron. Astrophys.* **2007**, *465*, 481–491. [CrossRef]
23. Liimets, T.; Corradi, R.L.M.; Jones, D.; Verro, K.; Santander-García, M.; Kolka, I.; Sidonio, M.; Kankare, E.; Kankare, J.; Pursimo, T.; et al. New insights into the outflows from R Aquarii. *Astron. Astrophys.* **2018**, *612*, A118.
24. Liimets, T. Nebulosities and Jets from Outbursting Evolved Stars. Ph.D. Thesis, University of Tartu, Tartu, Estonia, 2019. arXiv:1910.04157.
25. van Leeuwen, F. Validation of the new Hipparcos reduction. *Astron. Astrophys.* **2007**, *474*, 653–664. [CrossRef]
26. Liimets, T.; Corradi, R.M.L.; Jones, D.; Kolka, I.; Santander-Garcia, M.; Sidonio, M.; Verro, K. Nebulosities of the Symbiotic Binary R Aquarii—A Short Review. *Gold. Age Cataclysmic Var. Relat. Objects V* **2021**, *368*, 41.
27. Kraus, M.; Oksala, M.E.; Nickeler, D.H.; Muratore, M.F.; Borges Fernandes, M.; Aret, A.; Cidale, L.S.; de Wit, W.J. Molecular emission from GG Carinae's circumbinary disk. *Astron. Astrophys.* **2013**, *549*, A28.
28. Dobashi, K. Atlas and Catalog of Dark Clouds Based on the 2 Micron All Sky Survey. *Publ. Astron. Soc. Jpn.* **2011**, *63*, S1–S362. [CrossRef]
29. Fernandes, B.; Montmerle, T.; Santos-Silva, T.; Gregorio-Hetem, J. Runaways and shells around the CMa OB1 association. *Astron. Astrophys.* **2019**, *628*, A44.
30. Liu, H.B.; Takami, M.; Kudo, T.; Hashimoto, J.; Dong, R.; Vorobyov, E.I.; Pyo, T.S.; Fukagawa, M.; Tamura, M.; Henning, T.; et al. Circumstellar disks of the most vigorously accreting young stars. *Sci. Adv.* **2016**, *2*, e1500875.